IOP Conf. Series: Materials Science and Engineering **26** (2011) 012001 doi:10.1088/1757-899X/26/1/012001

# Manufacturing Ti-6Al-4V components by Shaped Metal Deposition: Microstructure and mechanical properties

**Bernd Baufeld[a*], Omer van der Biest[a], Rosemary Gault[b], and Keith Ridgway[b]**

[a]MTM, Katholieke Universiteit Leuven, Kasteelpark Arenberg 44, 3001 Leuven, Belgium

[b]AMRC, University of Sheffield, Advanced Manufacturing Park, Wallis Way, Catcliffe, Rotherham, S60 5TZ, UK

*corresponding author: b.baufeld@namrc.co.uk
Present affiliation: Nuclear AMRC, Brunel Way, Rotherham S60 5WG, UK

**Abstract**. The urge in aeronautics to reduce cost and time to flight of components without compromising safety and performance stimulates the investigation of novel manufacturing routes. Shaped Metal Deposition (SMD) is an innovative time-compression technology, which creates near-net shaped components layer by layer by weld deposition. Especially for Ti alloys, which are difficult to shape by traditional methods such as forging, machining and casting and for which the loss of material during the shaping process is also very expensive, SMD promises great advantages. Applying preliminary SMD parameter, four different tubular components with a square cross section and wall thicknesses of about 9 mm were built. The microstructure of the Ti-6Al-4V components consists of large prior β grains, elongated along the temperature gradient during welding, which transform into a lamellar α/β substructure at room temperature. The ultimate tensile strength was between 880 and 1054 MPa. The strain at failure was between 3.0 and 11.3 % for tensile testing parallel to the deposition plane and between 9.1 and 16.4 % perpendicular to the deposition plane. The micro-hardness (3.1 - 3.4 GPa), the Young´s modulus (117 - 121 GPa) and the oxygen and nitrogen content are comparable to cast Ti-6Al-4V material.

## 1. Introduction

Titanium alloys are increasingly applied in aeronautics achieving a weight proportion of about 10 wt.% in modern aircrafts [1]. The urge to reduce cost and time to flight of components without compromising safety and performance stimulates the investigation of novel manufacturing routes. Traditional methods to manufacture titanium alloy components usually are expensive due to the demanding machinability and the high material prices of titanium. Additive manufacturing, which reduces costs by omitting extensive machining and production of scrap, may be especially beneficial for the fabrication of complex shapes and small quantities. Several techniques of additive manufacturing are under investigation, including direct laser fabrication [2-11], electron beam freeform fabrication [12-14] and tungsten inert gas (TIG) welding [15-18]. The later is also called shaped metal deposition (SMD).

Titanium alloys are known for their sensitivity of the microstructure and of the mechanical properties on the thermal fabrication history [19-21]. Since the SMD process repeatedly subjects a component to high temperatures and high cooling rates, and since the layer by layer manufacturing results intrinsically to anisotropy, the microstructure of the SMD components are expected to be different to those prepared with conventional techniques. Hence, microstructure and mechanical properties of SMD components, their dependence on fabrication parameters and their competitiveness with conventionally fabricated material must be investigated. While some of these aspects already were discussed elsewhere [17, 18], in the present paper the influence of variation of deposition parameters on the mechanic properties are investigated.

## 2. Experimental details

### 2.1. Shaped metal deposition

The SMD cell consists of a TIG welding torch attached to a 6-axis Kuka robot which is linked to a 2-axis table. The welding material is supplied by a cold wire which is fed into the chamber through an annular feed pipe via a motorized roller guide ensuring a constant wire feed speed. In the present case, the TIG welding is performed with a Ti-6Al-4V wire with a diameter of 1.2 mm. Other wires, such as of stainless steel [22], ultra high strength low alloy steel [23], or Ni based superalloy In718 can also be applied. The welding is performed on a thick Ti-6Al-4V base plate fixed on the table.

The whole setup is enclosed in an airtight chamber filled with an inert gas (Ar, 99.999% purity) and the moisture is controlled. This allows to obtain a final product with low oxygen and nitrogen contamination (0.16 wt.% oxygen and 0.0041 wt.% nitrogen). These values are similar to the ones reported for the wire by the supplier (South Yorkshire Welding and Engineering Supplies): between 0.14 and 0.17 wt.% for oxygen and between 0.003 and 0.009 wt.% for nitrogen.

The controlling of the robot is performed by a CAD/CAM process where-by an off-line program provides the robot with the necessary weld path information. The whole process is controlled by an operator watching the weld through a water-cooled vision system which allows real-time monitoring of the weld, particularly the size of the bead and the weld pool and their distance from the contact tip.

Most important controlling parameters are the wire feed speed (WFS), the travel speed resulting from rotation and tilting of the table and the movement of the robot arm, the electrical current of the TIG welding, and the torch direction. Components reported in the present paper were created by depositing in a single track, rotating the table to keep a constant torch direction. Tubular components with a squared base (150x150 $mm^2$) were built (Figure 1). Four different components, A, B, C and D, were prepared with a variation of deposition parameters and component dimensions given in Table 1.

### 2.2. Tensile testing

Two different types of tensile specimens were prepared: A larger one with a gauge length of 35 mm and cross-section within the gauge length of 4×2 $mm^2$, and a smaller one with a gauge length of 10 mm and a cross-section within the gauge length of 3×2 $mm^2$ (for schematic drawings see Figure 1). The tensile direction of the larger specimens was parallel to the x direction of the components, while

**Table 1** Deposition parameters, the resulting geometry and mechanical properties of four different SMD components.

| | Deposition parameters | | | Geometry | | | Properties | |
|---|---|---|---|---|---|---|---|---|
| Component name | Current (A) | WFS (m/min) | travel speed (m/min) | Height (mm) | Wall width (mm) | Height of top region (mm) | µ-Vickers hardness (GPa) | Young´s modulus (GPa) |
| A | 150 | 2.1 | 0.30 | 120 | 8.8 | 8.8 | 3.1 | 117 |
| B | 183 | 2.2 | 0.25 | 70 | 9.5 | 8.7 | 3.2 | 118 |
| C | 163 | 1.8 | 0.30 | 70 | 8.8 | 8.2 | 3.3 | 121 |
| D | 165 | 1.4 | 0.25 | 70 | 9.5 | 8.8 | 3.4 | 118 |

the tensile direction of the smaller specimens was parallel to the z direction. The smaller tensile specimens comprise a tested region between 2 and 4 cm above the base plate. Some of the large specimens of component C were heat treated at 600°C for 2 h in a vacuum better than $6 \cdot 10^{-5}$ mbar.

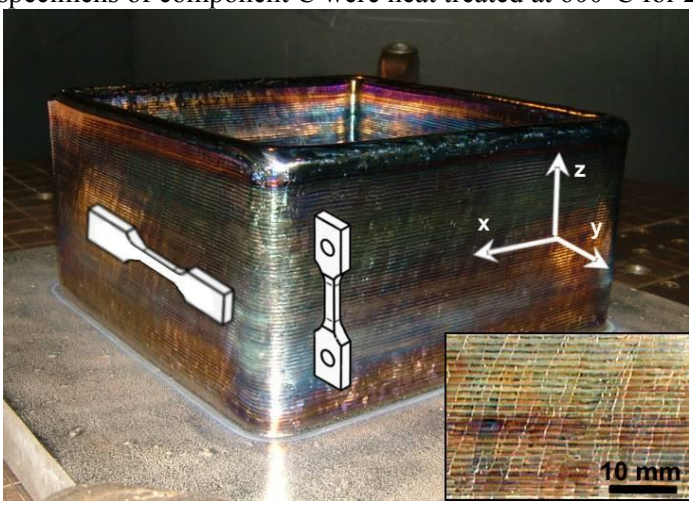


**Figure 1.** Component B with inset showing the magnified image of the wall surface. In addition, the coordinate system (x, y, z: directions of the welding head movement, wall thickness and height) and the orientation of the two different types of tensile specimens are exhibited schematically.

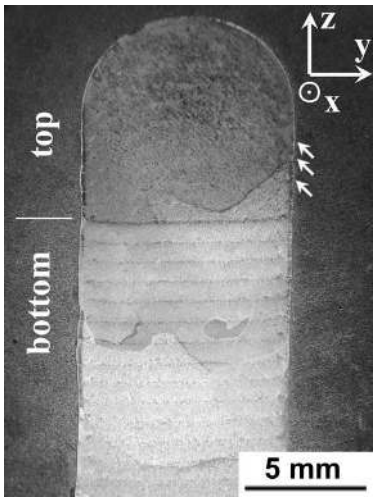


**Figure 2.** Etched cross-section of the upper part of component C exhibiting the top region without and the bottom region with parallel bands. Some of the weakly visible concave bands are indicated by arrows.

The different types of specimens were tested in two different Instron testing machines, both exhibiting a maximum load of 100 kN. The smaller specimens were tested with model TTDL with a displacement rate of 0.5 mm/min. The strain at fracture was determined by measuring the length of the two parts of the fractured specimens.

The larger specimens were tested with model 4505 under strain rate control, applying an extensometer with a gauge length of 25 mm. The strain rate usually was 0.15 mm/min; four specimens from component D however were tested at a higher strain rate of 1.50 mm/min. The strain at fracture of the larger specimens was determined from the plastic strain at fracture.

### 2.3. Characterization

The microstructure was investigated by optical and by scanning electron microscopy (SEM, FEI XL30FEG) of polished or etched cross sections. The etching agent was 6 vol.% nitrid acid and 3 vol.% hydrofluoric acid in water. Backscattered electron imaging with very high contrast allows discerning the $\alpha$ and $\beta$ phases without etching.

Vickers micro-hardness was measured with a Leitz micro-hardness tester with a load of 100 g on polished cross sections. A line of about 40 indents were performed on y-z planes from top towards the bottom in order to get reasonable statistics and information on possible changes over the component height. The dynamic Young's modulus of component was measured at room temperature by impulse excitation technique.

## 3. Results

### 3.1. Morphology and Microstructure

All investigated components exhibit similar features. The surfaces of the components, viewed from the side, show layered bulges parallel to the deposition plane and large, elongated grains (see inset of Figure 1). These elongated grains are prior $\beta$ grains which grew epitaxially across the welding layers.

They are inclined relative to the z direction, following the temperature gradient resulting from the moving welding torch. The layered bulges indicate the sequential deposition layers. The top of the components is round due to the surface tension of the melt.

Despite the high purity Ar atmosphere, some of the components have a colorized surface after manufacturing, indicating a very thin oxide layer. It is not yet understood, how to prevent this colorization. However, this colorization probably is just a cosmetic surface fault not degrading the mechanical properties, since in the bulk no increased oxygen concentration was observed.

The etched cross sections (y-z planes) exhibit aslant cut prior β grains and most obviously two different regions: a bottom region, which is characterized by bands parallel to the base plate, and a top region, where these parallel bands are absent (Figure 2b). The height of these top regions usually is the order of 8 to 9 mm (Table 1). The parallel bands are not related to the deposition layers [18].

In addition, convex bands (some indicated by arrows in Figure 2), much weaker in contrast than the parallel bands, can be observed throughout the whole component height. However, towards the bottom they are less visible. These convex bands generally end at the dent between two layered bulges at the wall surface. Especially noteworthy, the very top convex band ends at the wall surface dent between the top and the second top layer. Since this top layer indicates the melted material during the last SMD step, the convex bands can be related to the liquidus lines of the subsequent SMD steps. It must be stressed, that melted material may not only consist of the deposition material but also may include remelted material of previous depositions.

The microstructure in both regions consists of a Widmanstätten structure [20], which means α phase lamellae, forming basket weave or colony structures in a β matrix (Figure 3). Their morphology is different in both regions. The top region displays mostly colonies of parallel, very fine lamellae (Figure 3a), whereas the bottom region consists of much thicker lamellae (Figure 3b). Colonies habitually grow from prior β grain boundaries, which are still visible because they are decorated by an α phase ligament (not shown here) and from the wall surface (Figure 3a).

The different microstructure of the top and bottom region derives from the temperature gradient during subsequent SMD steps. To understand that, one has to know that Ti-6Al-4V exhibits a β phase field at high temperature and a α+β phase field at lower temperatures [19]. As described elsewhere [18], the top region represents the area which was within the β phase field during the very last SMD step. Because of the fast cooling after the last deposition, this region is in the two-phase field regime only for a short time, leading to fine α lamellae within a β matrix (Figure 3a). In contrast, the bottom region was subjected repeatedly to thermal treatments within the α+β phase field, which leads to a further diffusional partitioning of the α- and β-forming atoms and therefore to the coarsening (Figure 3b). The parallel bands (Figure 2) derive from the β/α+β transus lines of subsequent welding steps.

### 3.2. Tensile testing

The tensile deformation curves show extensive plastic deformation with limited work hardening

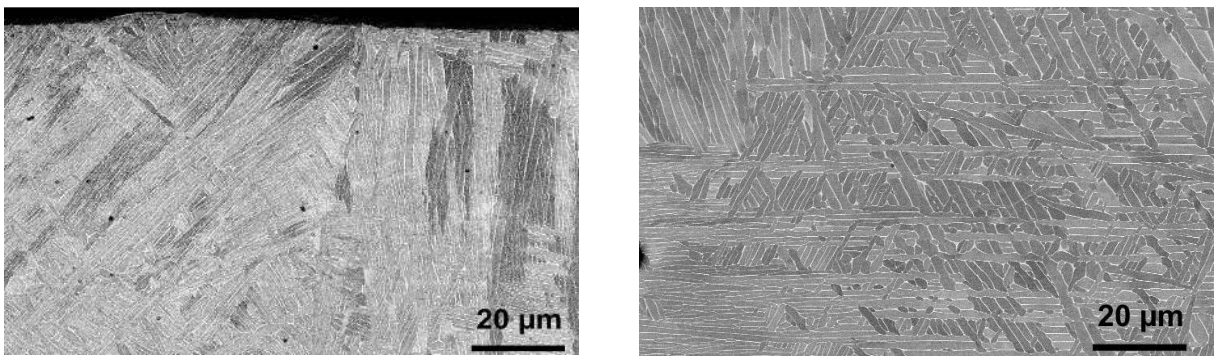


a) b)

Figure 3. Microstructures of component A from the top (a) and the bottom region (b) (y-z plane).

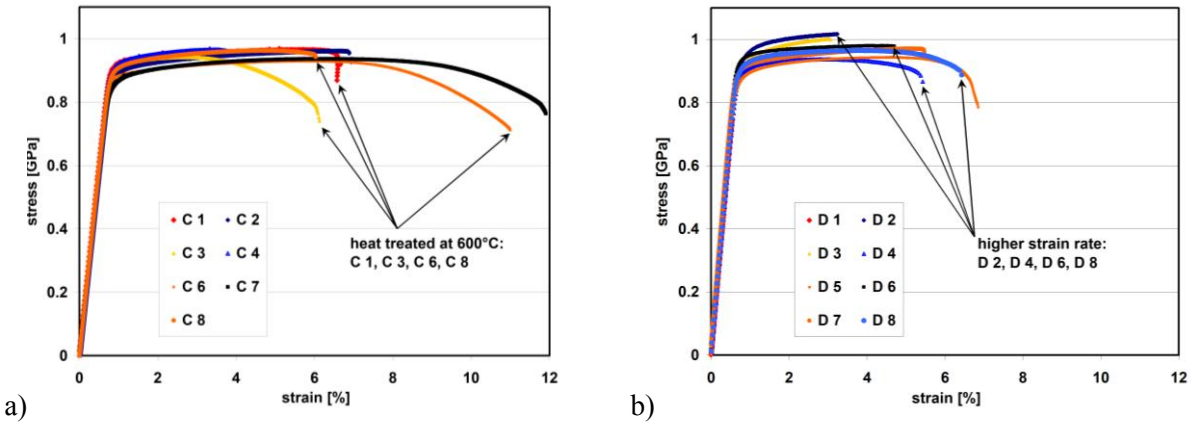


a) b)

**Figure 4**. Stress-strain curves for large tensile specimens from component C (a) and D (b). As indicated, some specimens were subjected to additional heat treatment (a) or to a higher strain rate.

(Figure 4). Some curves exhibit apparent softening due to necking (Figure 4, Figure 5). In Figure 4a, not only results are shown from as-prepared tensile specimens, but also from specimens heat treated at 600°C for 2 hours. However, no effect of the heat treatment can be discerned, neither for the occurrence of necking, the values and scatter of ultimate tensile strength (UTS), nor for the variations of strain at failure. The specimens also do not exhibit any strain rate sensitivity, as the comparison between tests with 0.15 mm/min and 1.50 mm/min show (Figure 4b).

In Figure 6, the UTS and the strain at failure are summarized for the large and for the small specimens. The UTS varies between 880 and 1054 MPa and the strain at failure between 3.0 and 16.4 %. On average the UTS of specimens from component A are smallest and from component D highest. No general trend can be found for relation of the UTS between small and large specimens. It is obvious, however, that the small specimens exhibit almost a threefold larger strain at failure than the large specimens. This may either be attributed to the difference in specimen size or to the difference in orientation. In the case of tensile SMD specimens with similar size, but different orientation it is also reported that the strain at failure is significantly larger for testing in z-direction of the component than in x-direction [17]. Therefore a size effect can be excluded. The orientation dependence of the strain at failure was attributed to the orientation of the elongated prior β grains [17], providing more grain boundaries, which are potential sites of failure, to the tensile specimens oriented in x-direction (in the present paper for the large specimens) than to specimens oriented in z-direction.

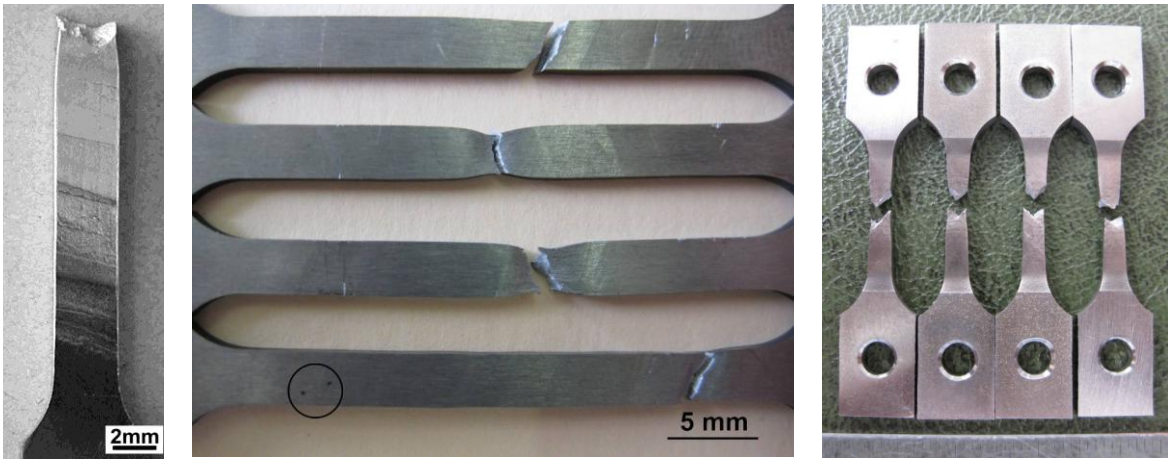


a) b) c)

**Figure 5**. Large specimens from component A (a) and B (b, heat treated) after fracture (x-y planes). Circle indicates pores. Small tensile specimen from component D (y-z planes) (c).

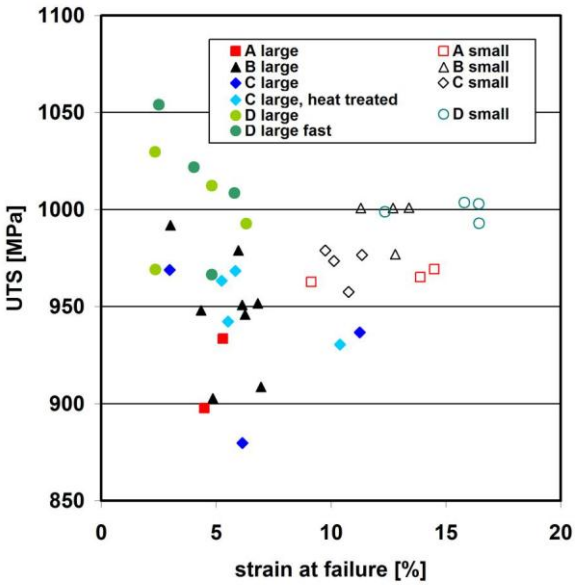


**Figure 6.** Summary of UTS and strain at failure of tested specimens from components A, B, C, and D, including results from heat treated specimens (C) and from tests with higher strain rate (D).

There is a certain scatter of the UTS and of the strain at failure within one set of specimens. The circle in Figure 5b directs the attention to the existence of pores. While not observed frequently, they may be the reason for the rather large variation of the UTS and the strain at failure; and of the appearance of necking which suggests stress concentration due to a reduced cross section.

After failure the surfaces of the x-y planes of the large specimens exhibit, despite being grinded before testing, a relief mimicking the prior β grains (Figure 5a). This relief apparently derives from slightly different preferential glide for the different prior β grains.

Naturally, the severe deformation significantly changes the microstructure. The α lamellae are lengthened and bended indicating their plasticity (Figure 7a). Pore formation at lamellae interfaces due to the deformations is also detected. The dimple structure of the fracture surface indicates plastic failure (Figure 7b).

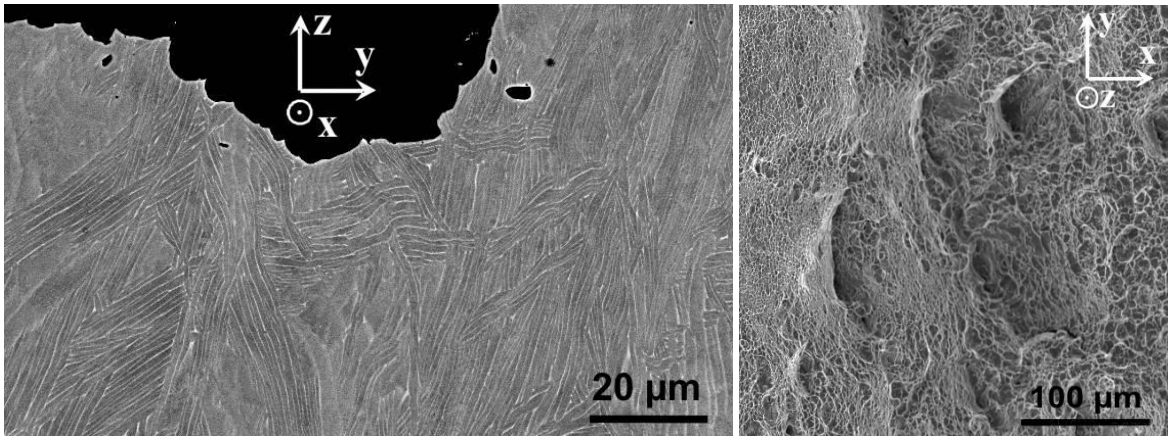


a) b)

**Figure 7.** Cross section at fracture site (a) and fracture surface (b) of small tensile specimens from component A

3.3. Other mechanic properties

The micro-hardness shows a certain scatter for all components, yet no dependence on the wall height (Figure 8). Also, the hardness in the top and in the bottom region does not differ. The average micro-hardness is given in Table 1. Apparently, the hardness increases slightly from 3.1 of component A to 3.4 of component D. This agrees with the finding that the UTS is lowest for component A and highest for component D. The Young´s modulus, also shown in Table 1, vary between 117 and 121 GPa, where component A exhibits the lowest and component C the highest value. Such a small variation however, probably is not of significance.

## 4. Conclusion

Net-shaped components can be fabricated by different sets of welding parameters. The UTS, hardness and Young´s modulus varies to some extent with the variation of welding parameters. However, not yet enough variations are investigated to conclude by which means the highest UTS, hardness or Young´s modulus can be obtained. Nevertheless, the mechanical properties are competitive to cast material with a low amount of oxygen and nitrogen contamination.

The strain at failure significantly depends on the orientation of the specimens exhibiting only values of about 5 % in direction parallel to the deposition plate, while perpendicular to the deposition plate strains at failure threefold as high are achieved. This should be kept in mind when designing the deposition routine addressing the orientation of the expected highest mechanical strain perpendicular to the deposition plane.

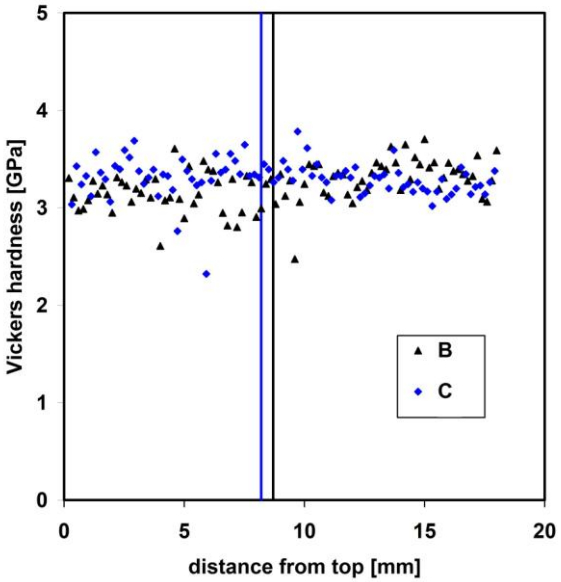


**Figure 8**. Vickers hardness (y-z plane) of component B (♦) and C (▲) vs. the distance from the top (z direction). The respective borders between top and bottom region are indicated.

**Acknowledgement**

The research is performed within the RAPOLAC STREP project under contract number 030953 of the 6th Framework Programme of the European Commission (www.RAPOLAC.eu), which is gratefully acknowledged.

**References**

[1] M. Peters & C. Leyens, *Titanium and Titanium Alloys,* Weinheim, Wiley-VCH, 2003, 513 pages
[2] P. A. Kobryn & S. L. Semiatin (2001) Mechanical Properties of Laser-Deposited Ti-6Al-4V. IN

D. L. Bourell, J. J. Beaman, R. H. Crawford, H. L. Marcus, L. Wood & J. W. Barlow (Eds.) *Solid Freeform Fabrication.* Austin, Tx, USA, The University of Texas at Austin
[3] X. Wu & J. Mei, Near net shape manufacturing of components using direct laser fabrication technology. *J. Mater. Process. Technol.,* Vol 135**,** 2003, p 266-270
[4] X. Wu, R. Sharman, J. Mei & W. Voice, Microstructure and properties of a laser fabricated burn-resistant Ti alloy. *Mater. Design,* Vol 25**,** 2004, p 103-109
[5] F. Wang, J. Mei & X. Wu, Microstructure study of direct laser fabricated Ti alloys using powder and wire. *Appl. Surf. Sci.,* Vol 253**,** 2006, p 1424-1430
[6] L. Qian, J. Mei, J. Liang & X. Wu, Influence of position and laser power on thermal history and microstructure of direct laser fabricated Ti-6Al-4V samples. *Mat. Sci. Tech.,* Vol 21**,** 2005, p 597-605
[7] S. Nowotny, S. Scharek, E. Beyer & K.-H. Richter, Laser Beam Build-Up Welding: Precision in Repair, Surface Cladding, and Direct 3D Metal Deposition. *J. Therm. Spray Tech.,* Vol 16**,** 2007, p 344-348
[8] F. Wang, J. Mei, H. Jiang & X. Wu, Laser fabrication of Ti6Al4V/TiC composites using simultaneous powder and wire feed. *Mat. Sci. Eng. A,* Vol 445-446**,** 2007, p 461-466
[9] S. H. Mok, G. Bi, J. Folkes & I. Pashby, Deposition of Ti-6Al-4V using a high power diode laser and wire, Part I: Investigation on the process characteristics. *Surf. Coat. Tech.,* Vol 202**,** 2008, p 3933-3939
[10] S. H. Mok, G. Bi, J. Folkes, I. Pashby & J. Segal, Deposition of Ti-6Al-4V using a high power diode laser and wire, Part II: Investigation on the mechanical properties. *Surf. Coat. Tech.,* Vol 202**,** 2008, p 4613-4619
[11] E. Brandl, C. Leyens, F. Palm, A. Schoberth & P. Onteniente (2008) Wire instead of powder? Properties of additive manufactured Ti-6Al-4V for aerospace applications. *Euro-uRapid.* Berlin, Germany, Fraunhofer-Allianz
[12] M. S. Domack, K. M. Taminger & M. Begley, Metallurgical mechanisms controlling mechanical properties of aluminum alloy 2219 produced by electron beam freeform fabrication. *Mat. Sci. Forum,* Vol 519-521**,** 2006, p 1291-1296
[13] K. M. Taminger & R. A. Hafley (2006) Electron Beam Freeform Fabrication for Cost Effective Near-Net Shape Manufacturing. *NATO/RTOAVT-139 Specialists' Meeting on Cost Effective Manufacture via Net Shape Processing.* Amsterdam, the Netherlands, NATO
[14] Arcam (2008) www.arcam.com.
[15] M. Katou, J. Oh, Y. Miyamoto, K. Matsuura & M. Kudoh, Freeform fabrication of titanium metal and intermetallic alloys by three-dimensional micro welding. *Mater. Design,* Vol 28**,** 2007, p 2093-2098
[16] D. Clark, M. Bache & M. Whittaker, Shaped metal deposition of a nickel alloy for aero engine applications. *J. Mater. Process. Technol.,* Vol 203**,** 2008, p 439-448
[17] B. Baufeld & O. Van der Biest, Mechanical properties of Ti-6Al-4V specimens produced by Shaped Metal Deposition. *Sci. Tech. Adv. Mat.,* Vol 10**,** 2009, p 10
[18] B. Baufeld, O. Van der Biest & R. Gault, Microstructure of Ti-6Al-4V specimens produced by Shaped Metal Deposition. *Int. J. Mat. Res.,* Vol. 100, 2009, p 1536-1542
[19] R. Boyer, G. Welsch & E. W. Collings, *Materials Properties Handbook: Titanium Alloys*, The Materials Information Society, 1994
[20] T. Ahmed & H. J. Rack, Phase transformations during cooling in α+β titanium alloys. *Mat. Sci. Eng. A,* Vol 243**,** 1998, p 206-211
[21] G. Lütjering, Influence of processing on microstructure and mechanical properties of (α+β) titanium alloys. *Mat. Sci. Eng. A,* Vol 243**,** 1998, p 32-45
[22] T. Skiba, B. Baufeld & O. Van der Biest, Microstructure and mechanical properties of stainless steel component manufactured by shaped metal deposition. *ISIJ Int.,* Vol 49**,** 2009, p 1588-1591
[23] T. Skiba, B. Baufeld & O. van der Biest, Shaped Metal Deposition of 300M Steel, Proc. IMechE Vol.225 Part B: J. Engineeering Manufacture, 2011, 831-839